

## Electronic Supporting Information

### **Intermetallic Pd<sub>3</sub>Pb Nanocubes with High Selectivity for the 4-Electron Oxygen Reduction Reaction Pathway**

Jocelyn T.L. Gamler,<sup>a</sup> Kihyun Shin,<sup>b</sup> Hannah M. Ashberry,<sup>a</sup> Yifan Chen,<sup>a,c</sup> Sandra L.A. Bueno,<sup>a</sup> Yawen Tang,<sup>c</sup> Graeme Henkelman,<sup>b</sup> and Sara E. Skrabalak<sup>a\*</sup>

---

<sup>a</sup> Department of Chemistry, Indiana University - Bloomington, 800 E. Kirkwood Ave. Bloomington, IN 47405, USA.

<sup>b</sup> Department of Chemistry and the Oden Institute for Computational Engineering and Science, The University of Texas at Austin- 105 E. 24<sup>th</sup> St., Stop A5300, Austin, TX, 78712, USA.

<sup>c</sup> Address here. Jiangsu Key Laboratory of New Power Batteries, Jiangsu Collaborative Innovation Center of Biomedical Functional Materials, School of Chemistry and Materials Science, Nanjing Normal University, Nanjing 210023, P. R. China.

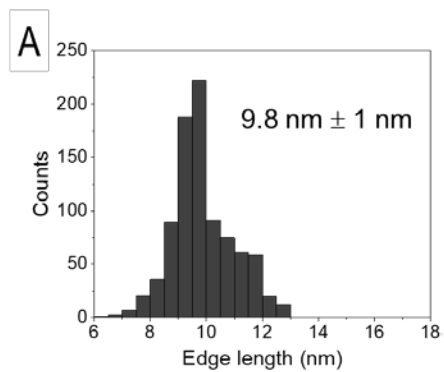


**Figure S1.** Size histogram for the sample shown in **Figure 1A**.

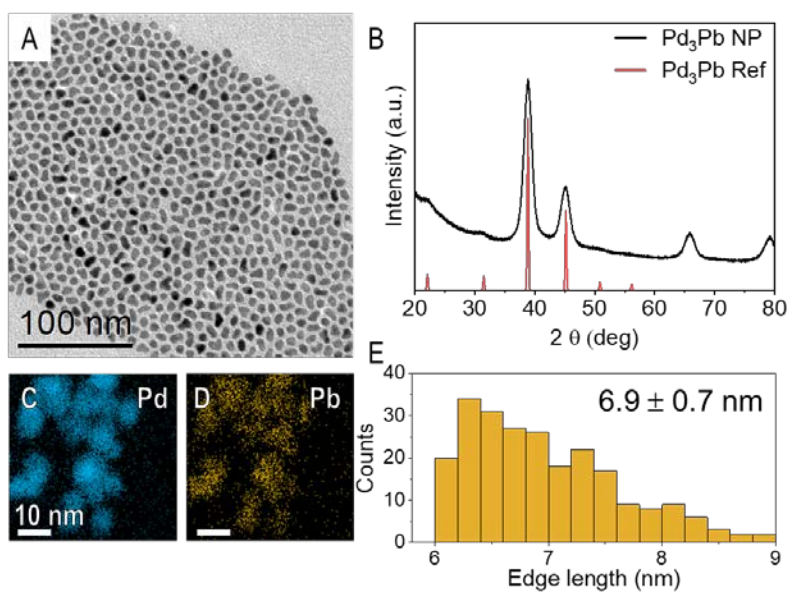


**Figure S2.** (A) TEM image, (B) XRD pattern, (C and D) STEM-EDX mapping and (E) histogram for the as-synthesized Pd<sub>3</sub>Pb NPs without TOP and OA.

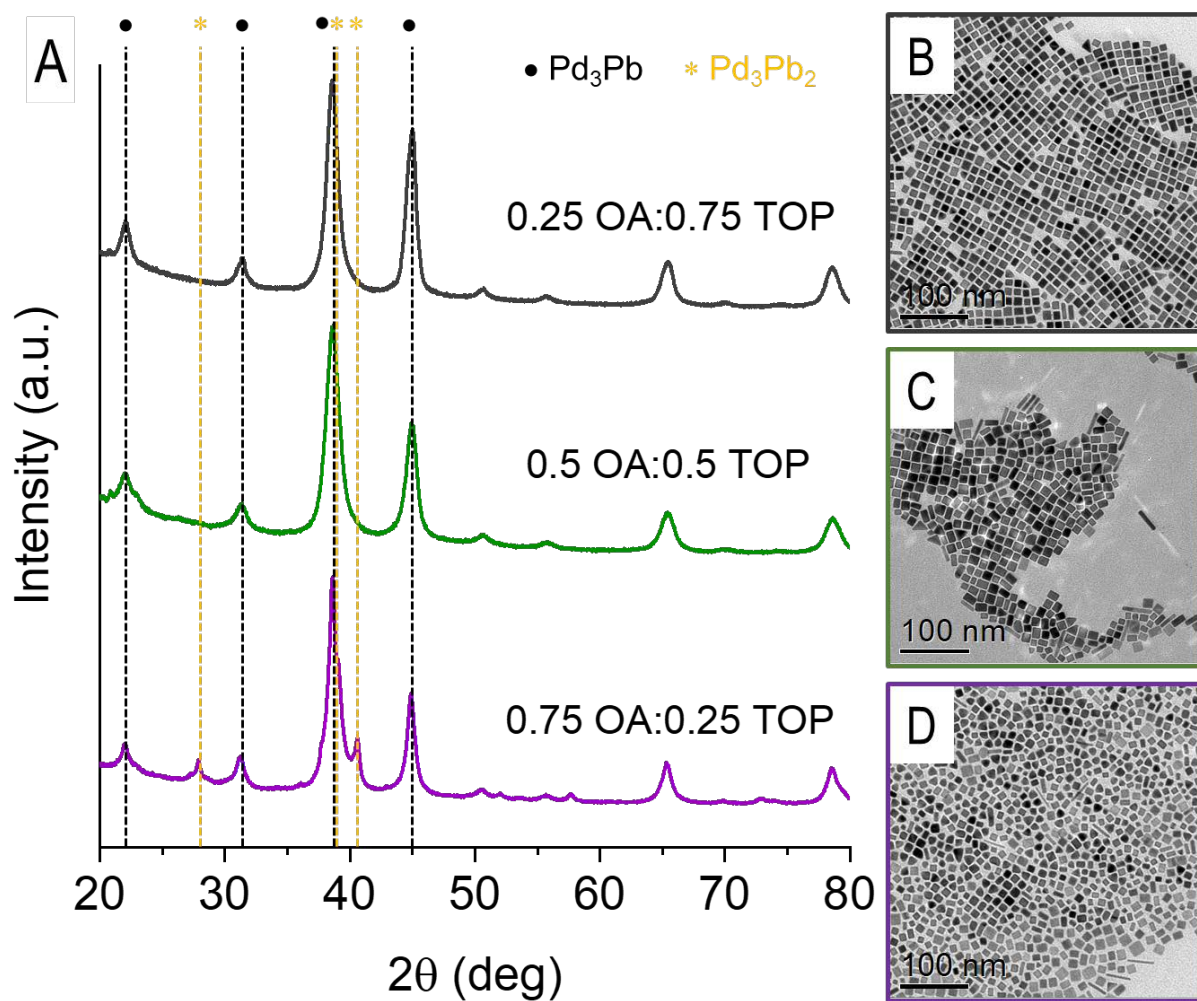


**Figure S3.** (A) XRD patterns and (C-D) corresponding TEM images for different OA:TOP ratios of 0.25:0.75, 0.5:0.5, and 0.75:0.25 for C-D, respectively. The black dashed lines indicate the intermetallic  $\text{Pd}_3\text{Pb}$  phase and the yellow dashed lines indicate the intermetallic  $\text{Pd}_3\text{Pb}_2$  phase.

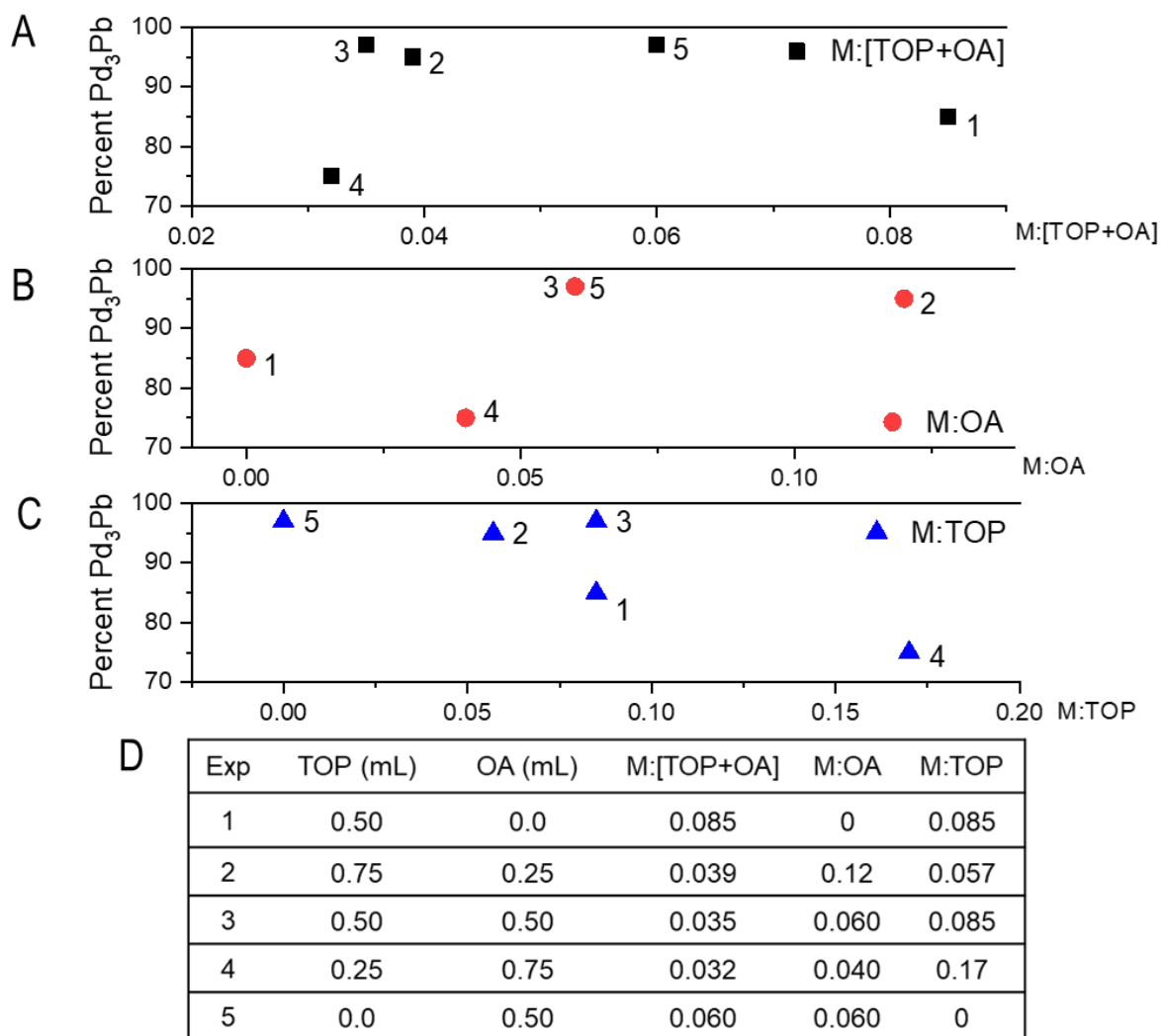


**Figure S4.** Plots of the relative molar ratios of (A) M:[TOP+OA], (B) M:OA, (C) M:TOP and (D) corresponding experimental conditions where the number next to each point references the experimental conditions listed in D. The percentage of  $Pb_3Pb$  intermetallic phase present in the XRD in **Figure 1B** where the other phase present is the  $Pd_3Pb_2$  crystal phase. The percentage of either phase cannot be 100 as we are forcing the existence of both phases and the two different Pd-Pb phases have peaks that overlap. Experiment 2 represents the optimized nanocubes synthetic parameters.

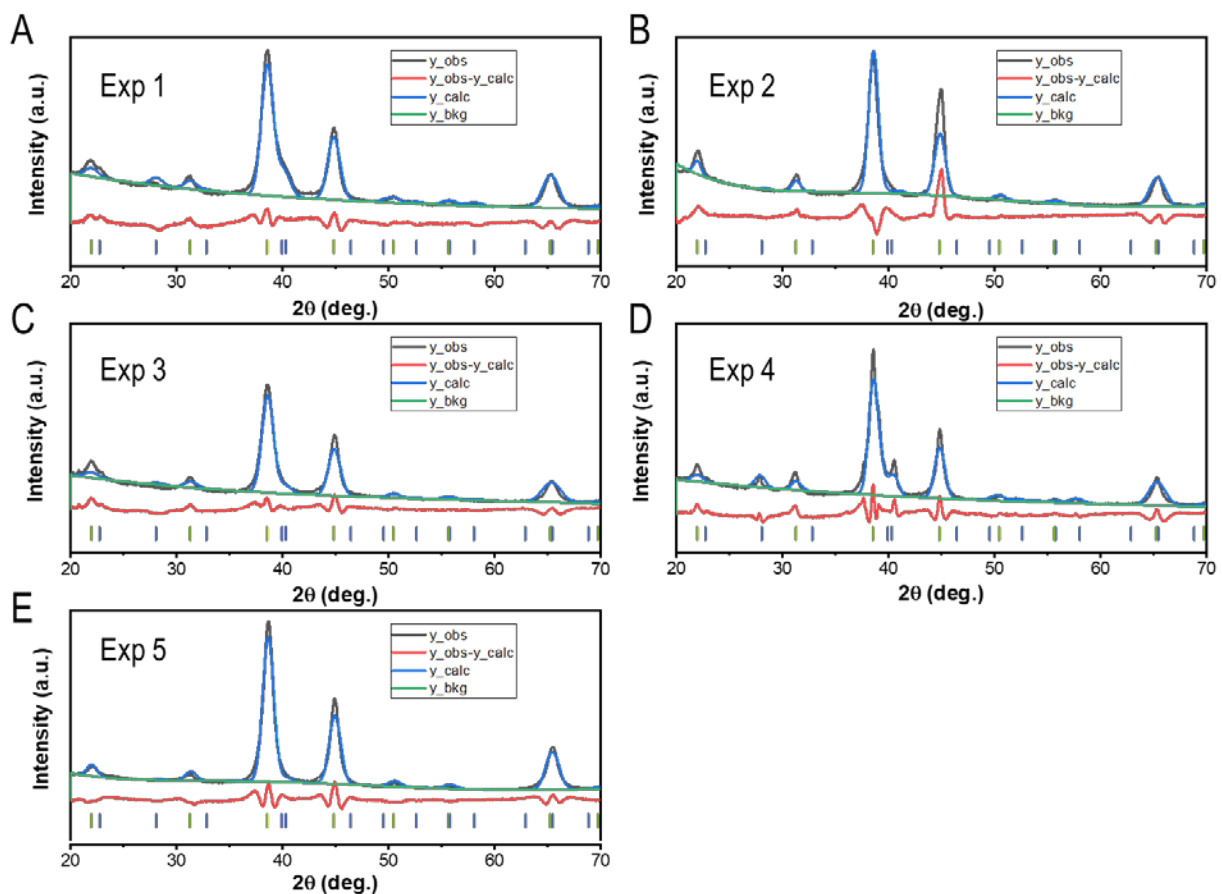


**Figure S5.** (A-E) Rietveld refinement to determine the percent of either the Pd<sub>3</sub>Pb or Pd<sub>3</sub>Pb<sub>2</sub> phase in the samples corresponding to Experiments 1-5, respectively, in **Figure S4D**. The black lines are the observed intensities, the blue lines are the calculated intensities, and the green lines are the background. The difference between the observed and calculated intensities are plotted in red. The ticks below the difference pattern correspond to the peaks of the two different phases, Pd<sub>3</sub>Pb (light green) or Pd<sub>3</sub>Pb<sub>2</sub> (purple). Rietveld refinement was performed with GSAS-II using Pd<sub>3</sub>Pb (ICSD 01-089-2062) and Pd<sub>3</sub>Pb<sub>2</sub> (ICSD collection code 197132) as the reference phases.

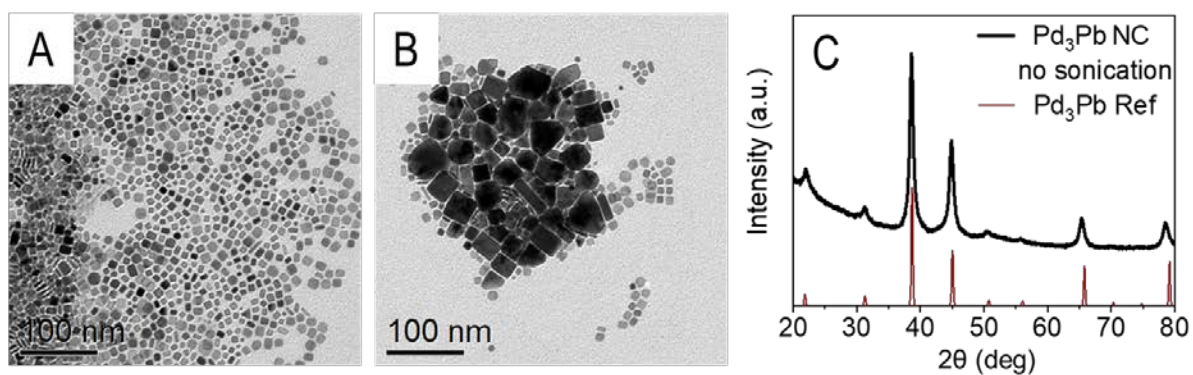


**Figure S6.** (A-B) TEM images of the products collected with a large size range and (C) XRD pattern when no sonication was used.

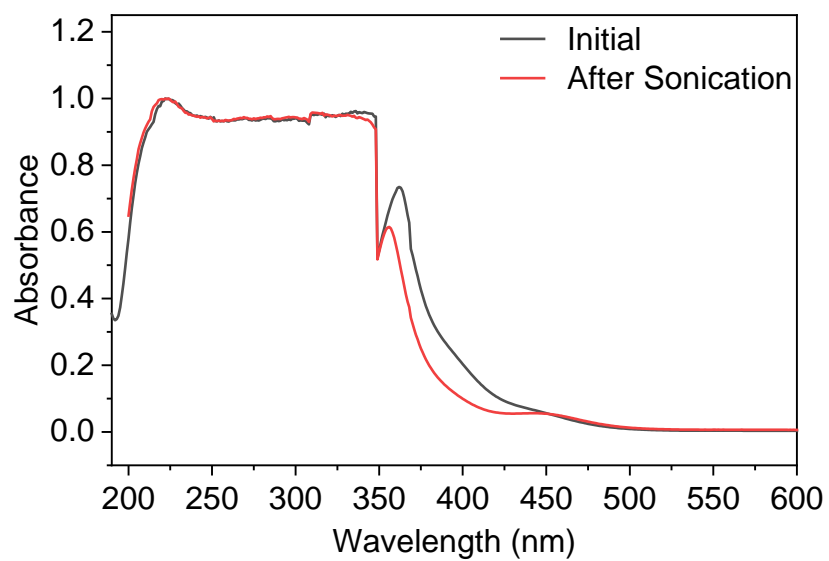


**Figure S7.** UV-visible spectra of the reaction solution before and after 30 minutes of sonication.

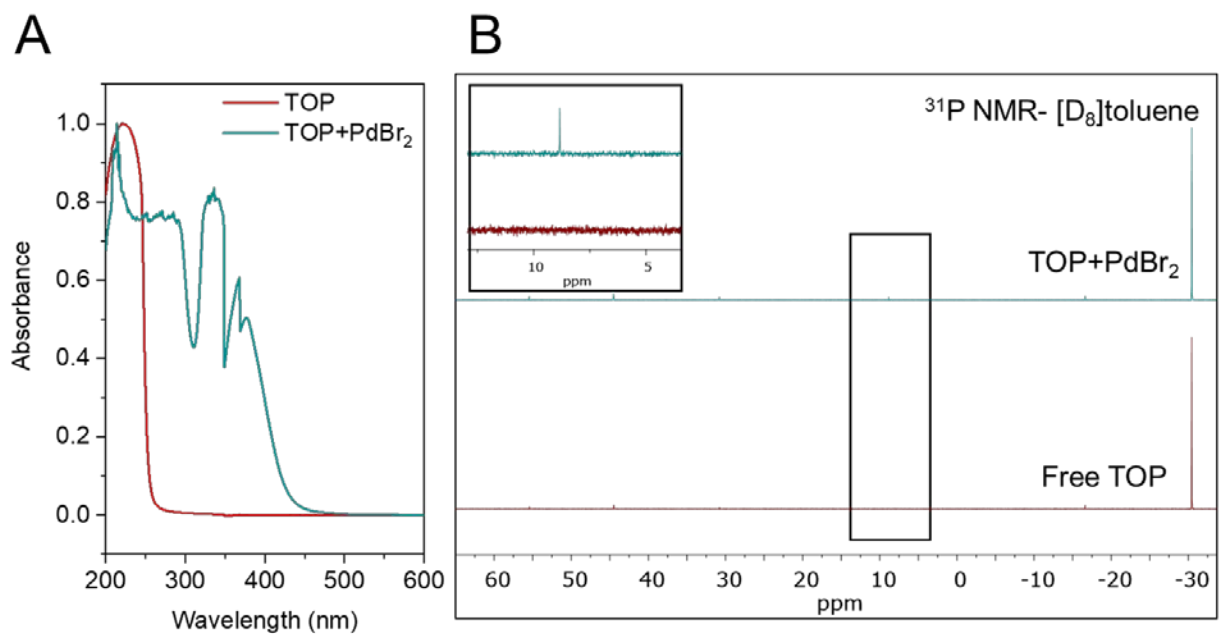


**Figure S8.** Characterization of TOP and PdBr<sub>2</sub> mixed with TOP by (A) UV-visible spectroscopy and (B) <sup>31</sup>P NMR in [D<sub>8</sub>]-toluene with inset showing the appearance of a peak with PdBr<sub>2</sub> is mixed with TOP.

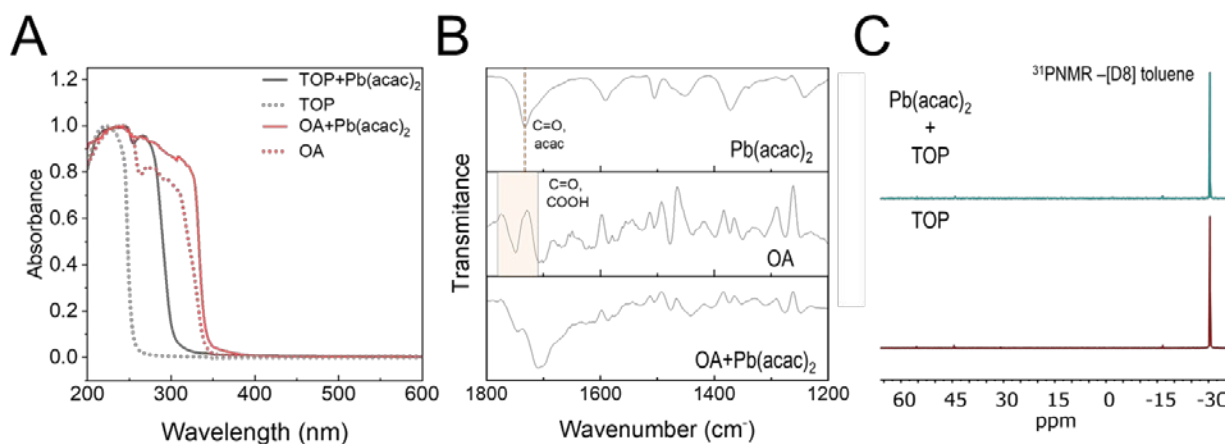


**Figure S9.** Characterization TOP, OA, TOP mixed with  $\text{Pb}(\text{acac})_2$ , and OA mixed with  $\text{Pb}(\text{acac})_2$  by (A) UV-visible spectroscopy. (B) FTIR characterization of  $\text{Pb}(\text{acac})_2$  mixed with OA where the orange dashed line indicated C=O stretch from acetylacetonate and the red shaded region C=O from the carboxylic acid from OA. (C)  $^{31}\text{P}$  NMR of (green, top)  $\text{Pb}(\text{acac})_2$  mixed with TOP and (red, bottom) pure TOP in  $[\text{D}_8]$ -toluene.

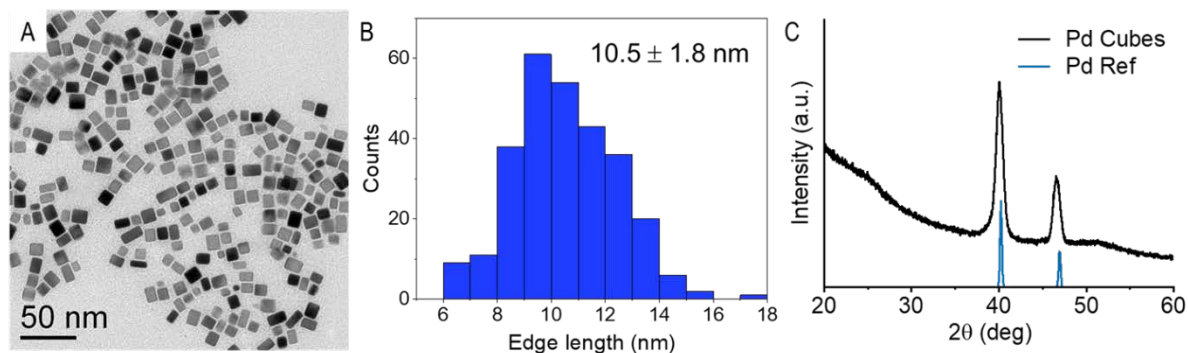


**Figure S10.** (A) TEM image of the Pd nanocubes used as a reference and corresponding (B) size histogram and (C) XRD pattern where the Pd reference is ICSD collection code 52251.

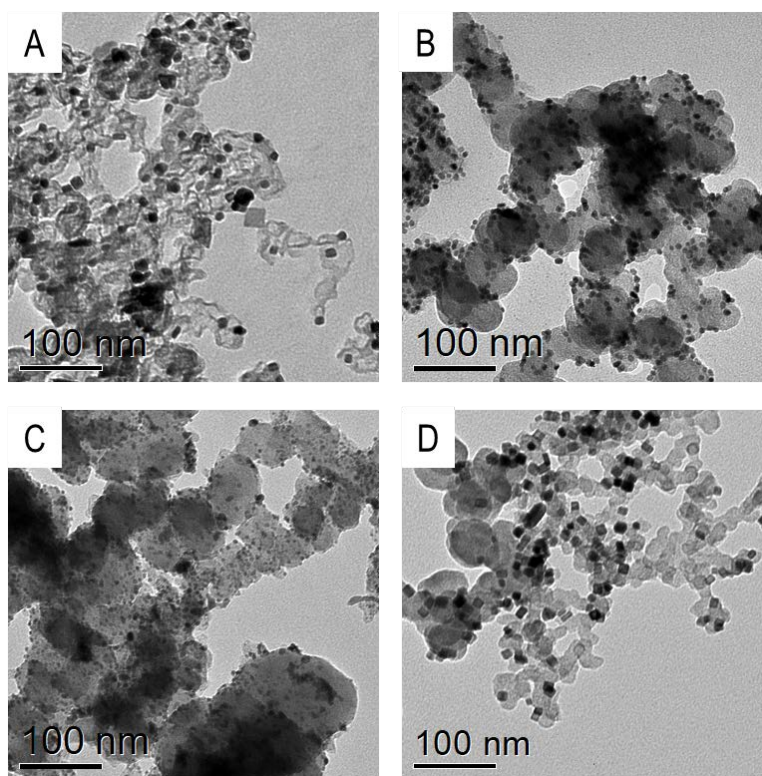


**Figure S11.** TEM images of the as-prepared catalysts for (A) Pd<sub>3</sub>Pb NC/C, (B) Pd<sub>3</sub>Pb NP/C, (C) commercial Pd/C, and (D) Pd NC/C.

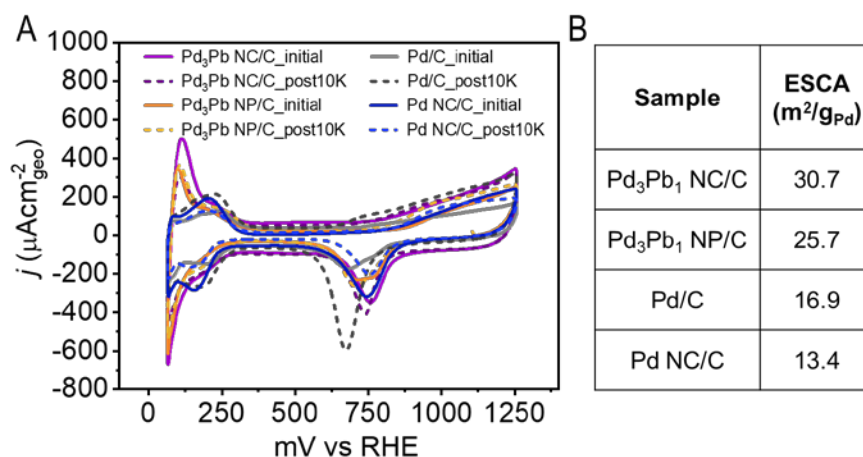


**Figure S12.** (A) Cyclic voltammograms collected in Ar-purged 0.1 M HClO<sub>4</sub> before and after ADT testing for each catalyst and (B) calculated electrochemically active surface area (ESCA).

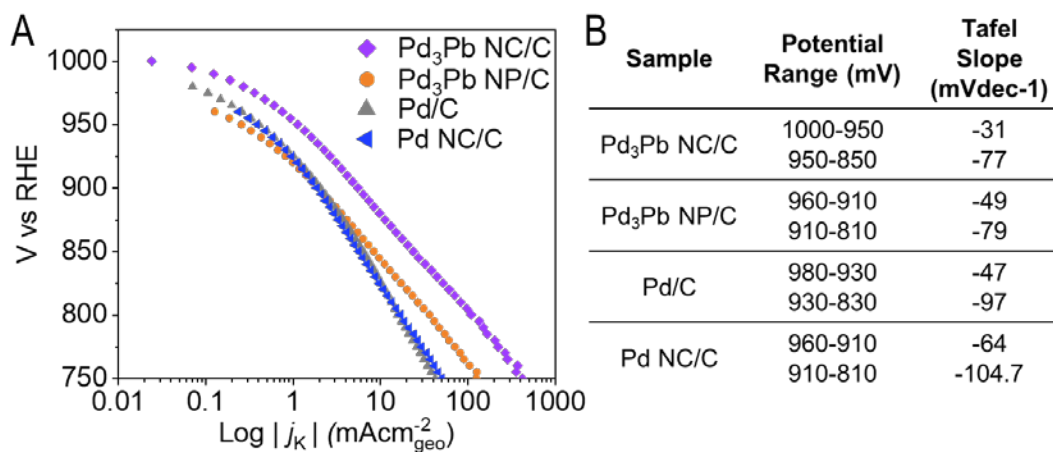


**Figure S13.** (A) Tafel plots for each catalysts and (B) corresponding Tafel slopes at listed potential ranges.

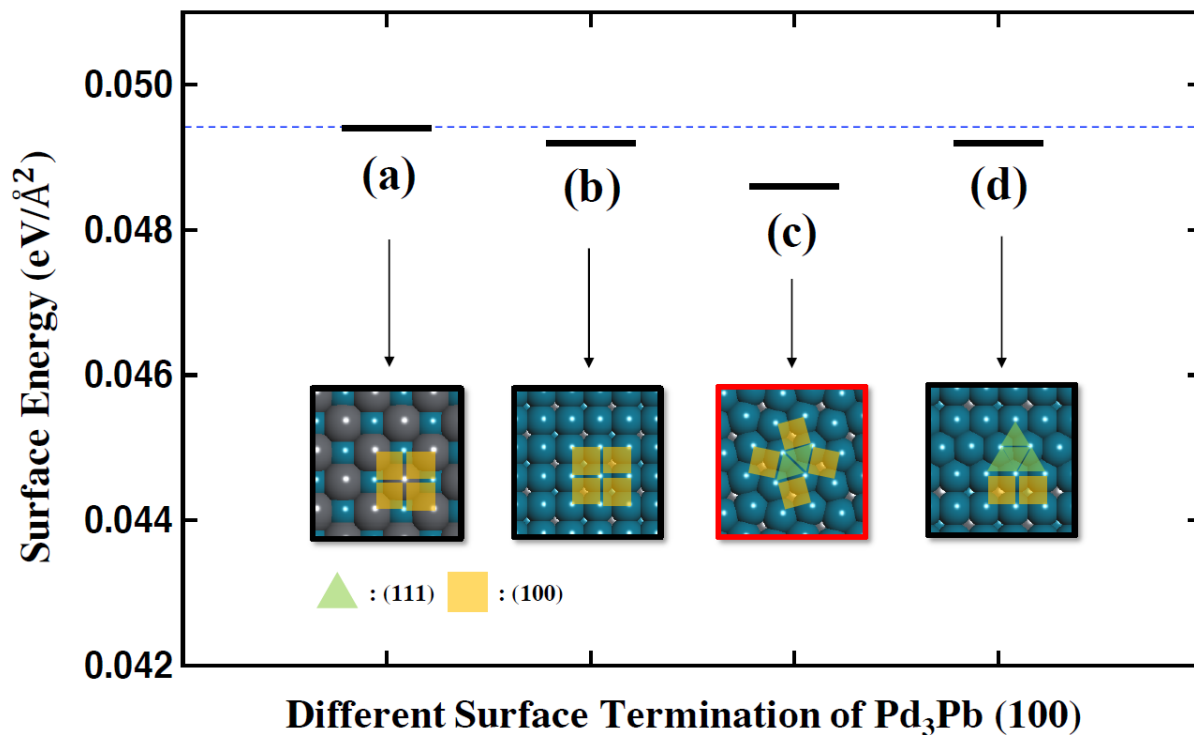


**Figure S14.** Different surface terminations were tested for Pd<sub>3</sub>Pb intermetallic (100). The grey atoms represent Pb and the blue atoms represent Pd. The different surface coordination are represented by the green triangle for (111) and the yellow square for (100). (a) Pd and Pb mixed termination, (b) only Pd termination with (100) facet, (c) (100) and (111) mixed, and (d) (100) and (111) mixed, but different ordering with (c).

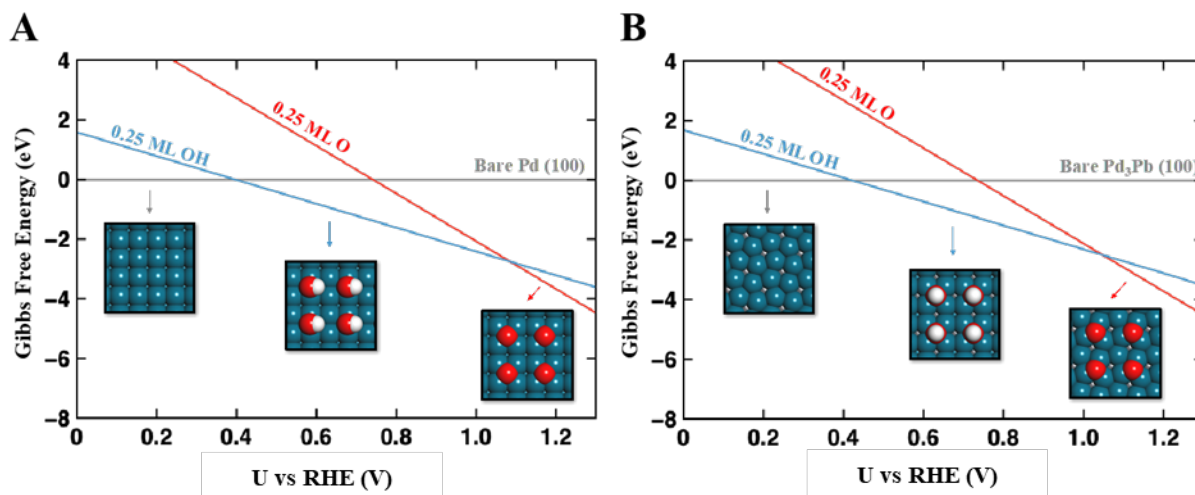


**Figure S15.** Surface Pourbaix diagrams for (A) Pd (100) and (B) Pd<sub>3</sub>Pb (100) surfaces. For both systems a 0.25 monolayer (ML) coverage is favorable for the experimental conditions and are used to determine the energy values in **Figure 4**.

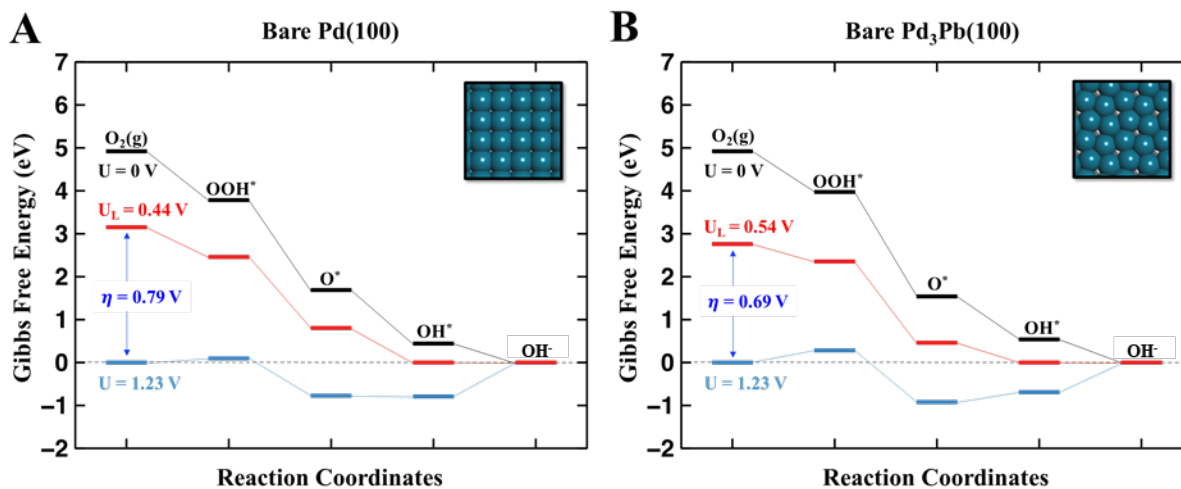


**Figure S16.** Gibbs free energy of the ORR reaction pathway for (A) Pd (100) and (B) Pd<sub>3</sub>Pb (100) surface where  $U_L$  (red) indicates the limiting potential and  $\eta$  indicates the overpotential ( $\eta = 1.23 - U_L$ ). Here, each surface is free of additional adsorbates.

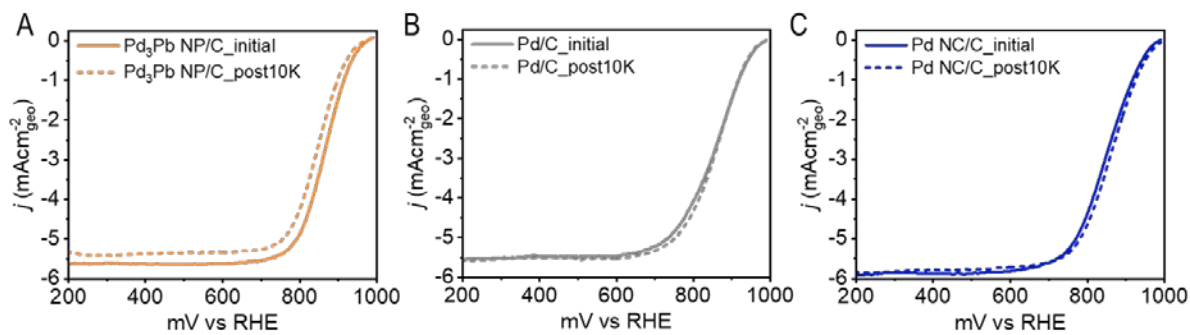


**Figure S17.** (A-C) Polarization curves before and after ADT collected in O<sub>2</sub>-saturated 0.1 M KOH at 1600 RPM for (A) Pd<sub>3</sub>Pb NP/C, (B) Pd/C, and (C) Pd NC/C

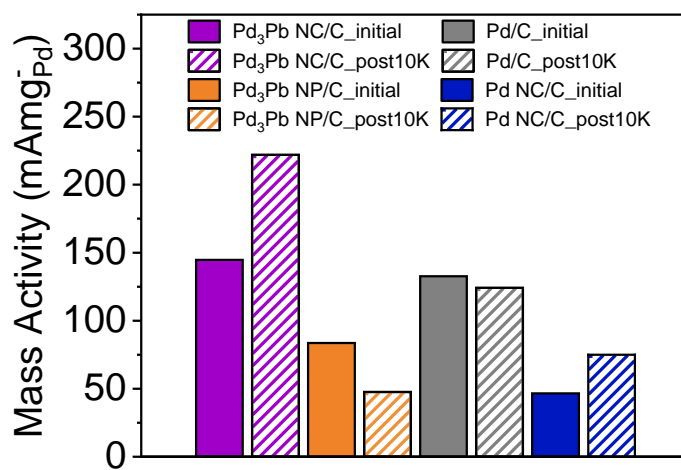


**Figure S18.** Mass activities for all tested catalysts before and after 10K cycles.

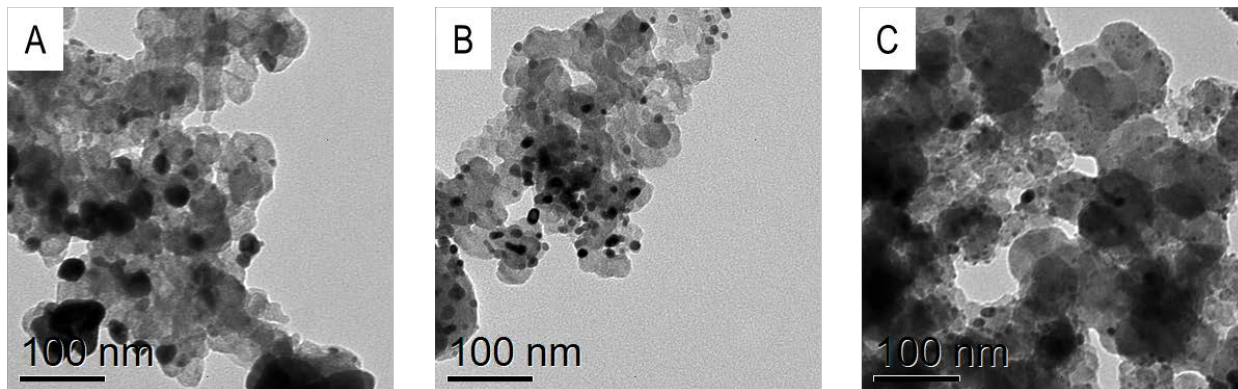


**Figure S19.** TEM images of the catalysts after ADT for (A) Pd<sub>3</sub>Pb NP/C, (B) Pd NC/C, (C) commercial Pd/C.

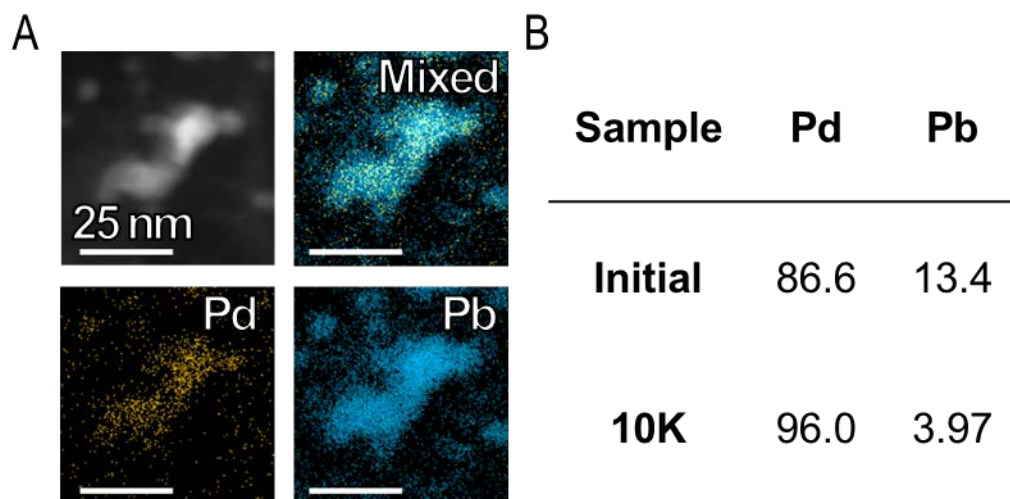


**Figure S20.** (A) STEM-EDX elemental mapping. (B) Summary of atomic amounts determined by EDX for the Pd<sub>3</sub>Pb NP before and after 10,000 durability cycles.

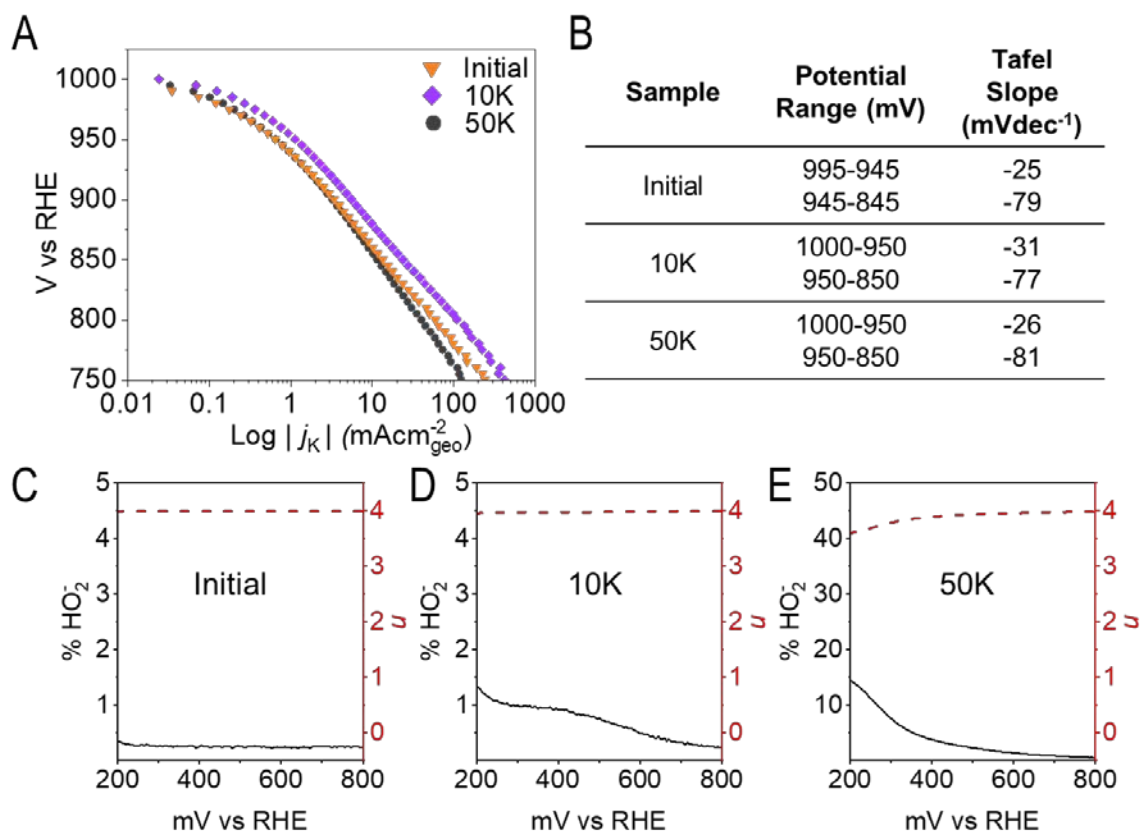


**Figure S21.** (A) Tafel plots for the Pd<sub>3</sub>Pb NC/C initially, after 10,000 and 50,000 potential cycles and (B) corresponding Tafel slopes at listed potential ranges. (C-D) Corresponding % HO<sub>2</sub><sup>-</sup> and electron transfer number (*n*) for initial, after 10,000 potential cycles, and after 50,000 potential cycles.

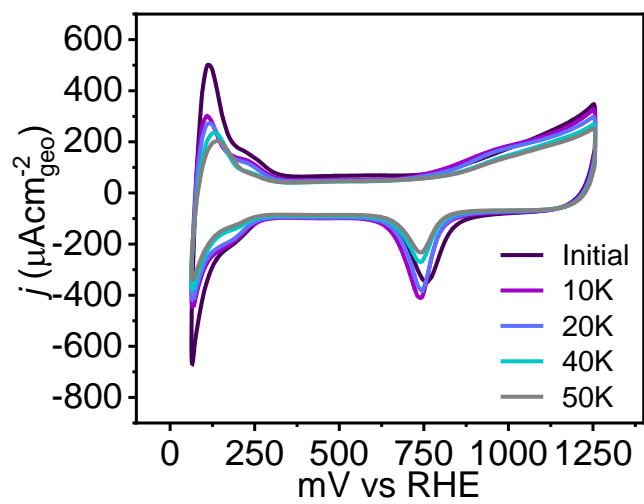


**Figure S22.** (A) Cyclic voltammograms collected in Ar-purges 0.1 M HClO<sub>4</sub> before and after 10K, 20K, 40K, and 50K cycles for Pd<sub>3</sub>Pb NC/C.

**Table S1.** Comparison of the ORR activity of Pd<sub>3</sub>Pb with other Pd-based electrocatalysts previously reported.

Electrocatalysts	Preparation	Size (nm)	Electrolyte	E <sub>1/2</sub> (V vs. RHE)	Ref
ordered Pd <sub>3</sub> Pb NC/C	low-temperature colloidal method	9.8	0.1 M KOH	0.880	This work
Pd <sub>3</sub> Pb NP/C	low-temperature colloidal method	6.9	0.1 M KOH	0.865	This work
Pd NC/C	Colloidal method	10.5	0.1 M KOH	0.860	This work
Pd/C	bought from Fuel Cell Store		0.1 M KOH	0.860	This work
ordered Pd <sub>3</sub> Pb NP/rGO-CNTs	gelation, freeze-dry, annealing	7.2	0.1 M KOH	0.862	1
ordered Pd <sub>3</sub> Pb NP/C	Co-reduction, annealing	5.2	0.1 M KOH	0.920	2
ordered Pd <sub>3</sub> Pb square nanoplates	low-temperature colloidal method	200	0.1 M KOH	0.887	3
Pt/C commercial	20 wt% Johnson-Matthey Corporation		0.1 M KOH	0.844	3
ordered PdCu NP	Co-reduction, annealing	5.1	0.1 M NaOH	0.857	4
ordered PdCuCo NP	Co-reduction, annealing	5.1	0.1 M NaOH	0.872	4
ordered PdCuNi NP	Co-reduction, annealing	5.1	0.1 M NaOH	0.862	4
Pd cube	low-temperature colloidal method	sub-10	0.1 M HClO <sub>4</sub>	0.860	5
Pd octahedra	low-temperature colloidal method	sub-10	0.1 M HClO <sub>4</sub>	0.805	5
Pd cube	low-temperature colloidal method	26.9	0.05 M H <sub>2</sub> SO <sub>4</sub>	0.87	6
Pd <sub>2</sub> NiAg	low-temperature colloidal method	15	0.1 M KOH	0.830*	7
FePd <sub>3</sub> NP/rGO	mixing, annealing	3.87	0.1 M KOH	0.750**	8
ordered Pd <sub>3</sub> Fe NP/C	mixing, annealing	7.5	0.1 M HClO <sub>4</sub>	0.767	9
Pt/C nanocubes	Colloidal method	12	0.1 M NaOH	0.834	10

Note: \* E<sub>vs RHE</sub> = E<sub>vs Ag/AgCl</sub> + 0.209 V + 0.059 × pH (Ag/AgCl in 3 M KCl)

\*\* E<sub>vs RHE</sub> = E<sub>vs SCE</sub> + 0.241 V + 0.059 × pH

## Reference

- 1) Fu, G.; Liu, Y.; Wu, Z.; Lee, J.-M. *ACS Appl. Nano Mater.* 2018, **1**, 1904-1911.
- 2) Cui, Z.; Chen, H.; Zhao, M.; DiSalvo, F. J. *Nano Lett.* 2016, **16**, 2560-2566.
- 3) Wang, K.; Qin, Y.; Lv, F.; Li, M.; Liu, Q.; Lin, F.; Feng, J.; Yang, C.; Gao, P.; Guo, S. *Small Methods* 2018, **2**, 1700331.
- 4) Jiang, K.; Wang, P.; Guo, S.; Zhang, X.; Shen, X.; Lu, G.; Su, D.; Huang, X. *Angew. Chem., Int. Ed.* 2016, **55**, 9030-9035.
- 5) Shao, M.; Odell, J.; Humbert, M.; Yu, T.; Xia, Y. *J. Phys. Chem. C* 2013, **117**, 4172-4180.
- 6) Erikson, H.; Sarapuu, A.; Alexeyeva, N.; Tammeveski, K.; Solla-Gullón, J.; Feliu, J. M. *Electrochim. Acta* 2012, **59**, 329-335.
- 7) Liu, S.; Zhang, Q.; Li, Y.; Han, M.; Gu, L.; Nan, C.; Bao, J.; Dai, Z. *J. Am. Chem. Soc.* 2015, **137**, 2820-2823.
- 8) Yin, H.; Liu, S.; Zhang, C.; Bao, J.; Zheng, Y.; Han, M.; Dai, Z. *ACS Appl. Mater. Interfaces* 2014, **6**, 2086-2094.
- 9) Meku, E.; Du, C.; Sun, Y.; Du, L.; Wang, Y.; Yin, G. *J. Electrochem. Soc.* 2016, **163**, 132-138.
- 10) R. Devivaraprasad, R. Ramesh, N. Naresh, T. Kar, R. K. Singh and M. Neergat, *Langmuir*, 2014, **30**, 8995–9006.